

The Crystal Structure of Yeast Phenylalanine tRNA at 2.0 Å Resolution: Cleavage by Mg²⁺ in 15-year Old Crystals

Luca Jovine, Snezana Djordjevic and Daniela Rhodes*

MRC Laboratory of Molecular Biology, Hills Road, Cambridge CB2 2QH, UK

We have re-determined the crystal structure of yeast tRNA^{Phe} to 2.0 Å resolution using 15 year old crystals. The accuracy of the new structure, due both to higher resolution data and formerly unavailable refinement methods, consolidates the previous structural information, but also reveals novel details. In particular, the water structure around the tightly bound Mg²⁺ is now clearly resolved, and hence provides more accurate information on the geometry of the magnesium-binding sites and the role of water molecules in coordinating the metal ions to the tRNA. We have assigned a total of ten magnesium ions and identified a partly conserved geometry for high-affinity Mg²⁺ binding. In the electron density map there is also clear density for a spermine molecule binding in the major groove of the TΨC arm and also contacting a symmetry-related tRNA molecule. Interestingly, we have also found that two specific regions of the tRNA in the crystals are partially cleaved. The sites of hydrolysis are within the D and anticodon loops in the vicinity of Mg²⁺.

© 2000 Academic Press

*Corresponding author

Keywords: tRNA^{Phe}; crystal structure; Mg²⁺; spermine; RNA hydrolysis

Introduction

Transfer RNAs (tRNAs) decode the genetic information in messenger RNA and carry amino acid residues to the ribosome where protein synthesis takes place. The availability from cells and their great biological importance rendered tRNAs the target of early crystallographic studies on nucleic acid structure. The three-dimensional structure of yeast phenylalanine tRNA was independently determined by two groups a quarter of a century ago to 3.0 Å resolution (Robertus *et al.*, 1974; Kim *et al.*, 1974), and subsequently the resolution was extended to 2.5 Å (Ladner *et al.*, 1975; Quigley *et al.*, 1978). Since at that time there was no direct structural information on DNA, the crystal structure of yeast tRNA^{Phe} provided the first view of nucleic acid double helices, and, more interestingly, it revealed the complexity of RNA folding, together with a wealth of information on how this is achieved. The structure showed how the “clover-

leaf” secondary structure of tRNAs folds into a compact L-shaped three-dimensional structure held together by a set of tertiary and triple base-pair interactions, as well as a number of magnesium ions that are crucial for folding and stability (Figure 1(a), (b)) (Ladner *et al.*, 1975; Jack *et al.*, 1977; Quigley *et al.*, 1978; Stout *et al.*, 1978; Westhof *et al.*, 1988a).

The crystallographic work on yeast tRNA^{Phe} also provided the first structural information on site-specific self-cleavage of an RNA molecule and the role of divalent metal ions in the hydrolysis (Brown *et al.*, 1983, 1985). This preceded the discovery of ribozymes, RNA enzymes that catalyse the specific cleavage and formation of chemical bonds (Cech & Uhlenbeck, 1994; Scott & Klug, 1996). In yeast tRNA^{Phe}, a specifically bound Pb²⁺ causes the rapid and specific hydrolysis of the RNA chain between residues H2U17 and G18 in the D loop, both in solution and in the crystal at neutral pH conditions (Brown *et al.*, 1983, 1985). From this work it was concluded that the Pb²⁺ participates directly in the reaction by acting as a base catalyst involving metal-hydrate complexes, and that an in-line attack mechanism may be involved. Site-specific hydrolysis of tRNA can also take place in solution in the presence of Mg²⁺, but in this case optimal cleavage rates require elevated tempera-

Present address: L. Jovine, Department of Biochemistry and Molecular Biology, Mount Sinai School of Medicine, 1 Gustave L. Levy Place, New York, NY 10029-6574, USA.

E-mail address of the corresponding author: rhodes@mrc.lmb.cam.ac.uk

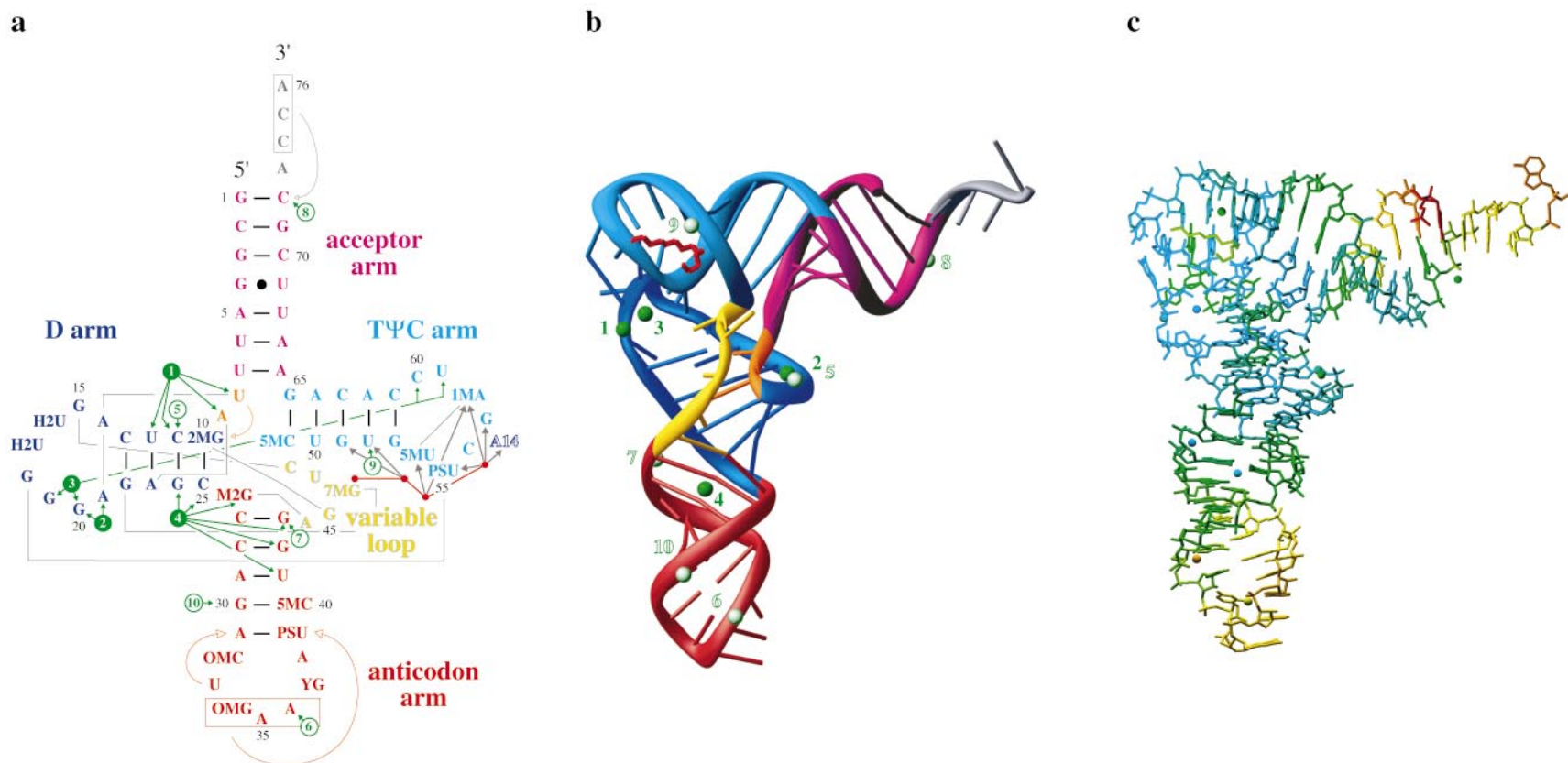


Figure 1. The location of Mg²⁺ in the secondary and tertiary structure of yeast tRNA^{Phe}. (a) "Cloverleaf" representation of yeast tRNA^{Phe} secondary structure. Different regions of the molecule are indicated and colour-coded accordingly. Watson-Crick base-pairs are represented by short black lines, the single G4·U69 wobble pair is marked by a black dot. Tertiary interactions are shown as grey lines, while arrows indicate stacking of the enclosed nucleotides onto 5' or 3' helices. The anticodon and the terminal CCA sequence are boxed in red and grey, respectively. Tightly and weakly bound Mg²⁺ are shown as green and white circles, respectively, with green arrows indicating the nucleotides with which they interact. The spermine molecule is represented by a red stick, with four dots corresponding to its nitrogen atoms (not drawn to scale); grey arrows indicate interactions with the RNA. The A14 nucleotide of a symmetry-related molecule is labelled in reverse colours. Modified nucleotide name abbreviations are; 2MG, N2-methylguanosine; H2U, dihydrouridine; M2G, N2,N2-dimethylguanosine; OMC, 2'-O-methylcytidine; OMG, 2'-O-methylguanosine; YG, wybutosine; PSU, pseudouridine; 5MC, 5-methylcytidine; 7MG, 7-methylguanosine; 5MU, ribosylthymine; 1MA, 1-methyladenosine. (b) Ribbon representation of the three-dimensional structure. The structure is colour coded as in (a). Tightly and weakly bound Mg²⁺ are shown as dark and pale green circles, respectively, and indicated by their respective numbers. The spermine molecule, in red, is shown in stick representation. Water molecules have been omitted for clarity. (c) Stick representation of the three-dimensional structure, colour-coded according to temperature factors. Temperature factors from low to high are depicted on a scale going from blue to red, respectively. The most flexible regions of the structure are the 5' strand of the acceptor stem, the terminal CCA sequence and the anticodon loop. Nucleotides H2U16 and H2U17 are also highly mobile, but this is not as evident in this Figure because their occupancy was refined to account for the Mg²⁺-catalysed cleavage (see Materials and Methods).

tures and high pH conditions (Wintermeyer & Zachau, 1973).

The recent interest in RNA structure and self-cleaving ribozymes, together with the development of intense X-ray sources, as well as modern structure refinement methods, prompted us to re-examine the crystals of yeast tRNA^{Phe} with the aim of obtaining higher resolution and more accurate structural information than was possible 25 years ago. The structure we have determined at 2.0 Å resolution consolidates the previous structural information, but also reveals novel details on the geometry of the Mg²⁺ binding sites and the role of the inner and outer hydration shells in coordinating the metal. We have assigned ten Mg²⁺ and there is also clear density for a spermine molecule contacting two symmetry-related tRNA molecules in the crystal lattice. Interestingly, we have also found that the tRNA in the 15-year old crystals is partially and specifically cleaved in two regions of the RNA chain, both in the vicinity of Mg²⁺ ions. The positions of cleavage are in the D loop, between G15, H2U16 and H2U16, H2U17, and within the anticodon loop. We discuss the possible mechanism for the magnesium-dependent cleavage of tRNA and its relationship to the previously observed cleavage by lead.

Results and Discussion

The crystals used in this study for re-determining the three-dimensional structure of yeast tRNA^{Phe} were about 15 years old and of the same type (monoclinic, space group P2₁) as the ones used for the determination of the original crystal structure by our group (Ladner *et al.*, 1972, 1975; Robertus *et al.*, 1974; Jack *et al.*, 1977). The crystals, which had been grown using the dialysis method, had been stored at 4 °C. Despite their age, they preserved excellent order and diffracted to beyond 2.0 Å resolution at the ESRF synchrotron source at 100 K. Interestingly, the age of the crystals allowed partial and apparently magnesium-dependent site-specific hydrolysis within two regions of the RNA chain.

Structure determination and overall model

The structure of yeast tRNA^{Phe} (76 nucleotides) was solved to 2.0 Å resolution as described in Materials and Methods. The current model has been refined to an *R* factor of 22.7% and a *R*_{free} of 26.3%, and includes ten Mg²⁺ ions, one spermine molecule and 220 water molecules (Table 1). The quality of the resulting electron density map can be seen in Figures 2 and 3. Figure 1(a) and (b) show the well known “cloverleaf” representation of yeast tRNA^{Phe} secondary structure and its L-shaped three-dimensional fold, together with the location of the Mg²⁺ and the spermine molecule. The new structure corroborates essentially all of the major features of tRNA obtained from previous structural analyses (Ladner *et al.*, 1975; Jack *et al.*,

Table 1. Crystallographic data collection and refinement statistics

A. Crystallographic data	
Number of crystals	1
Temperature (K)	100
Space group	P2 ₁
	<i>a</i> = 55.25, <i>b</i> = 32.99, <i>c</i> = 61.88, β = 90.38
Unit cell dimensions (Å)	
Resolution range (Å)	25.80–2.00
Wavelength (Å)	0.932
Number of reflections	30,638
Number of unique reflections	13,678
Completeness (%)	88.6 (70.7) ^a
Redundancy	3.1 (2.6) ^a
(<i>I</i> / σ(<i>I</i>))	14.8 (2.2) ^a
<i>R</i> _{sym} (%) ^b	3.6 (17.1) ^a
B. Refinement	
Number of atoms	1912 (76 nt, 10 Mg ²⁺ , 1 spermine, 220 H ₂ O)
<i>R</i> value (%)	22.7 (34.0) ^d
<i>R</i> _{free} (%) ^c	26.3 (41.3) ^d
Bond length deviation (Å)	0.0088
Bond angle deviation (deg.)	1.4
Improper angle deviation (deg.)	1.3
Dihedral angle deviation (deg.)	12.7
Average <i>B</i> factor (Å ²)	53.6
Minimum <i>B</i> factor (Å ²)	14.9
Maximum <i>B</i> factor (Å ²)	120.9
<i>B</i> RMSD for bonded main-chain atoms (Å ²)	3.5
<i>B</i> RMSD for bonded side-chain atoms (Å ²)	4.1

^a Values in parenthesis refer to the highest resolution shell (2.10–2.00 Å).

^b $R_{\text{sym}} = \sum_h \sum_i |I_i(h) - \langle I(h) \rangle| / \sum_h \sum_i I_i(h)$, where $I_i(h)$ is the *i*th measurement and $\langle I(h) \rangle$ is the mean of all measurements of $I(h)$ for Miller indices *h*.

^c *R*_{free} is the *R* value obtained for a test set of reflections, consisting of a randomly selected 6.8% subset (926 reflections) of the diffraction data, not used during refinement.

^d Values in parenthesis refer to the highest resolution shell (2.07–2.00 Å).

1977; Quigley *et al.*, 1978; Stout *et al.*, 1978; Westhof *et al.*, 1988a) with a root mean square deviation (RMSD) between the new and old structures of ~1.1 Å (see Materials and Methods), but also provides novel insights. The most interesting new findings are the identification of a conserved coordination geometry between magnesium ions and RNA and the location of a spermine molecule sandwiched between two tRNA molecules. In addition, the ribose puckers of nucleotides A21 and U47 have been modified to C3'-endo and C2'-endo, respectively; the conformation of nucleotide G19 has been changed to anti; the 3'-end nucleotide A76 does not continue the stacking of the C atoms in the CCA-end, but instead points in the opposite direction, interacting with A36 of an adjoining tRNA molecule.

The crystal structure colour-coded according to temperature factors in Figure 1(c) shows, strikingly, that the most rigid part of the structure is the central region where the D and TΨC loop interact, and also where the variable loop and the linker between acceptor and D stems come together by

a

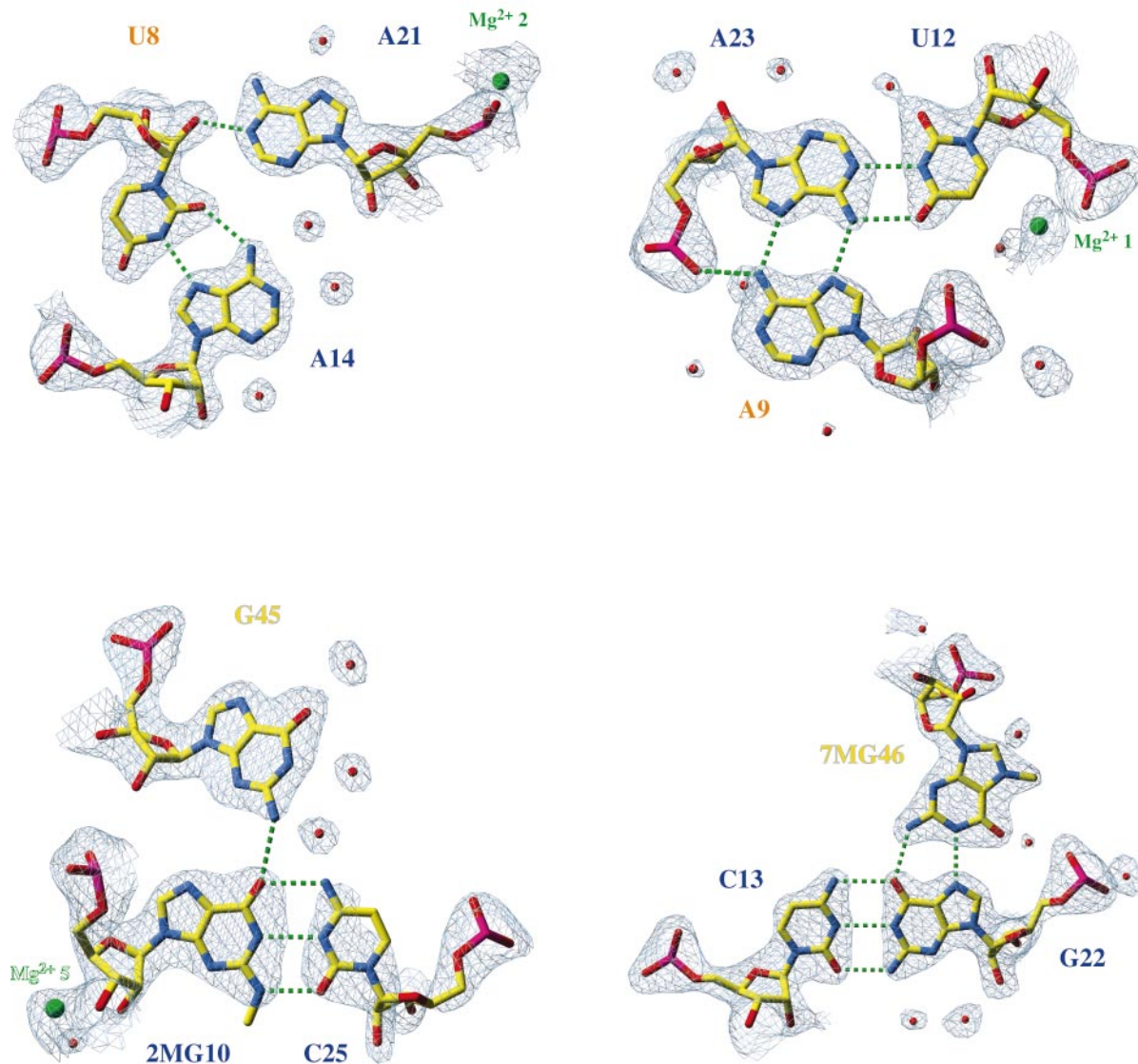


Figure 2 (legend opposite)

forming both tertiary base-pairs and triple base-pairs with the D stem and its linker to the anticodon arm (Jack *et al.*, 1976; Quigley *et al.*, 1978; Westhof & Sundaralingam, 1986). Consequently, the most complex part of the structure is more rigid than the double helical stems of the acceptor and anticodon arms. The most flexible parts of the structure are the 5' strand of the acceptor stem, the CCA-end, a short single stranded stretch of the D loop containing the two dihydrouridine groups and the anticodon loop. The rigid, central region of the structure contains four tightly bound Mg²⁺ ions, binding sites 1, 2, 3 and 4 (Figures 1(a), (b)

and 3). All these Mg²⁺ have low temperature factors, confirming that they are important for stabilising the three-dimensional fold. This is particularly evident in the case of Mg²⁺ 3 and 4, which, due to an extensive network of both direct and water-mediated contacts, have lower temperature factors than the RNA nucleotides with which they interact (Figure 3(c), (d)). This observation is consistent with solution melting studies on yeast tRNA^{Phe} that show that removal of Mg²⁺ lowers the melting temperature and changes the melting pathway (Rhodes, 1977). However, since the overall structure of yeast tRNA^{Phe} is approximately the

b

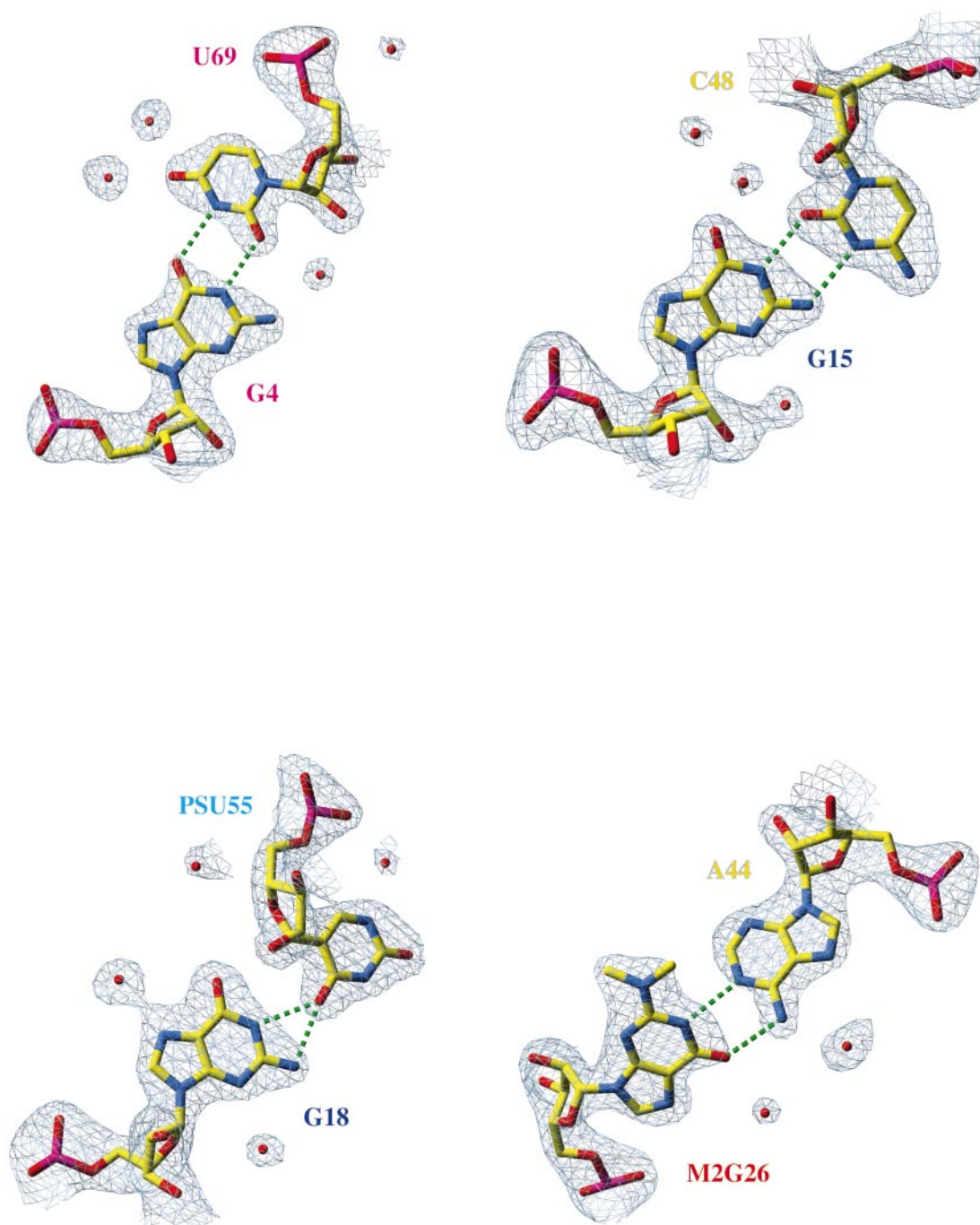


Figure 2. Gallery of triple and tertiary base-pairs in the three-dimensional structure of yeast tRNA^{Phe}. (a) Stick representation of triple base-pairs shown within their combined, sigma-weighted $|2F_o - F_c|$ electron density map contoured at 1.0σ . Phosphate atoms are shown in magenta, carbon atoms in yellow, nitrogen atoms in blue and oxygen atoms in red. Nucleotide labels are colour coded according to the scheme in Figure 1(a). Mg^{2+} and water molecules are indicated by green and red spheres, respectively. For clarity, only hydrogen bonds between nucleotides are shown (broken green lines). (b) Stick representation of tertiary base-pairs shown within their combined, sigma-weighted $|2F_o - F_c|$ electron density map contoured at 1.0σ . Conventions are as in (a).

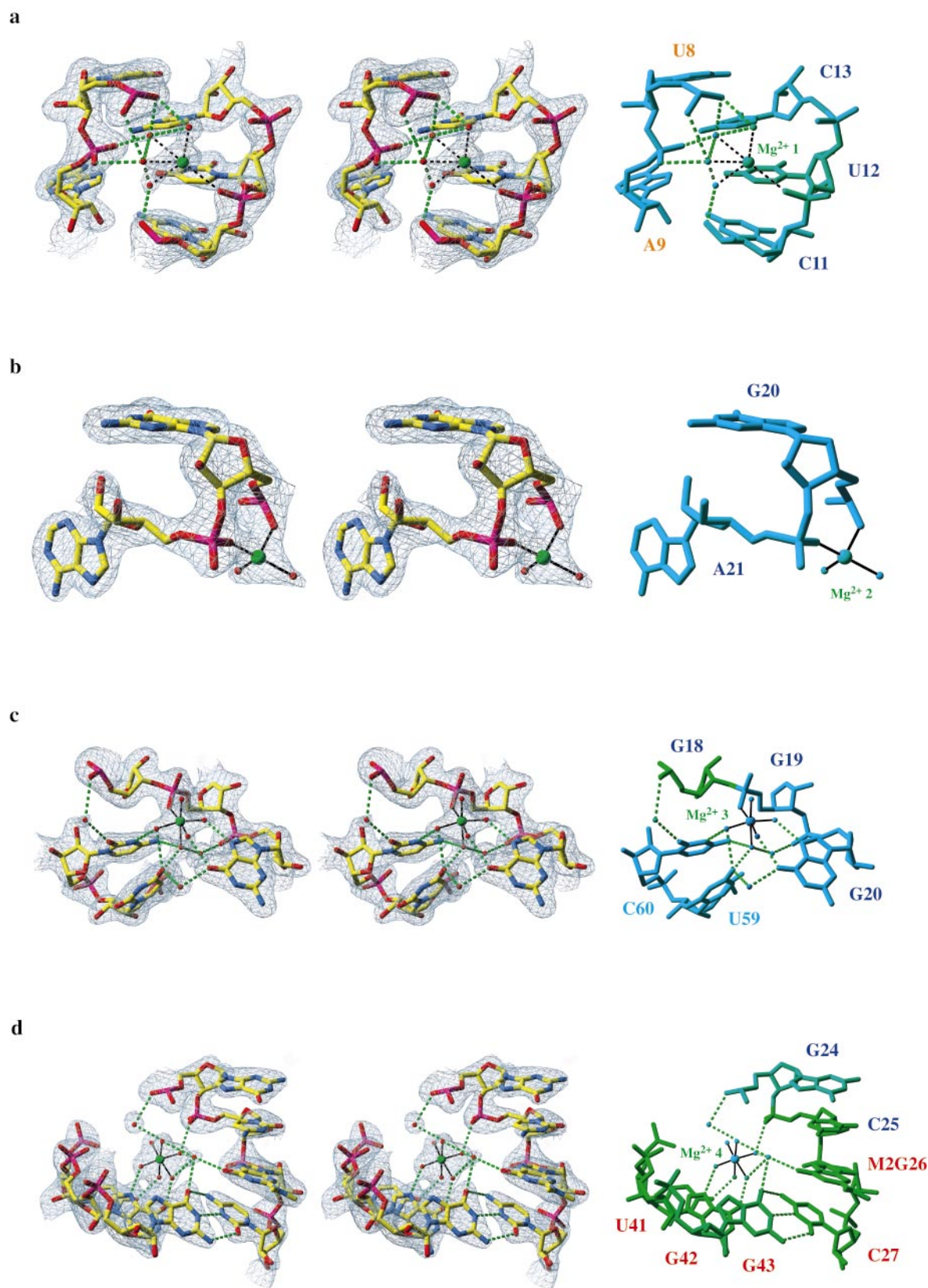


Figure 3. The four-strong Mg^{2+} -binding sites in yeast *tRNA^{Phe}*. (a) Mg^{2+} -binding site 1, (b) Mg^{2+} -binding site 2, (c) Mg^{2+} -binding site 3, (d) Mg^{2+} -binding site 4. For each site, a stereo representation with combined, sigma-weighted $|2F_o - F_c|$ electron density map contoured at 1.0 σ is shown on the left; on the right, the same binding sites are shown colour-coded according to temperature factors. Conventions are as described in legend to Figure 2. Direct bonds (≤ 2.1 Å) involving Mg^{2+} ions are shown as continuous black lines, with the exception of the longer range contacts made by Mg^{2+} 1 (a), which are depicted as broken black lines. The bases of nucleotides G18 and G19 have been omitted for clarity from (c).

same in 0.1 M NaCl as it is in 10 mM MgCl₂ (Rhodes, 1977), the folding of the “cloverleaf” into the three-dimensional structure must be driven by the formation of tertiary base-pairs rather than by the binding of Mg²⁺. The folding therefore creates the binding pockets for the magnesium ions that in turn bind and tighten up the structure becoming integral parts of the architecture, as is apparent from their low temperature factors. In addition to this important structural role, Mg²⁺ ions can be essential for RNA folding as is the case in, for instance, the *Tetrahymena* group I intron P4-P6 domain in which folding of the RNA nucleates around a Mg²⁺ core (Cate *et al.*, 1996; 1997; Feig & Uhlenbeck, 1999).

Non-canonical and triple base-pairs

Figure 2 shows a gallery of all triple and tertiary base-pairs found in yeast tRNA^{Phe}. These have been noted before in the three-dimensional structure of yeast tRNA^{Phe} and also in that of other tRNAs, but the high resolution of the present structure permits the hydration around these unusual base-pair interactions to be seen directly. Certain patterns of hydration are recurring features, such as water molecules within hydrogen bonding distance of the O6 or N7 of non-Watson-Crick base-paired guanine bases (Westhof 1988; Auffinger & Westhof, 1997).

Water structure

Although the water structure of the new model was completely rebuilt, the general solvent distribution reflects those of the previous studies (Westhof *et al.*, 1988b), with the highly ordered corner of the L-shaped tRNA displaying the highest levels of concentration of water molecules. More than 80% of the water molecules we have assigned interact directly with RNA atoms; interestingly, almost 60% of these interactions are made with the nucleic acid backbone, reflecting the involvement of a high proportion of functional groups on the bases in both secondary and tertiary pairs. About 14% of the RNA-bound water molecules are bridging either adjacent or non-adjacent phosphate oxygen atoms, with 4% contacting both oxygen atoms of single phosphate groups. In addition, almost 10% of the water molecules are bridging the ribose O2' and either the N3 of purines or the O2 of pyrimidines (see for example nucleotides A14, A23 (Figure 2(a)) and G15, C48, U69 (Figure 2(b))). Concerning interactions between water molecules and RNA bases, there is an overall preference for guanine nucleotides (almost 45% of the observed contacts). In the case of purines, the groups more frequently involved are the N6 and N3 of adenine nucleotides and the O6 and N2 of guanine nucleotides, while an approximately equal proportion of interactions are observed at the O2 and N4/O4 positions of pyrimidines.

Binding sites for Mg²⁺ and spermine

We have assigned ten Mg²⁺ binding sites and one spermine molecule (Figures 1(a), (b), 3 and 4). Six of the Mg²⁺ have relatively high temperature factors (up to about 105 Å² in the case of Mg²⁺ 10) and/or only partial occupancies (as low as about 1/3 for Mg²⁺ 7); they bind directly to the oxygen atoms of phosphate groups and some also interact with the O3' of a neighbouring ribose (Mg²⁺ 5 and 8). Presumably, the negative charge of other phosphate groups within the tRNA molecule is neutralised by additional Mg²⁺, but these are too mobile to be observed in the electron density map. Four magnesium ions are very tightly bound (*B* factors ~30-50 Å²), occupying unique geometric environments in the three-dimensional fold of the tRNA (Figure 3). Three of these sites (Mg²⁺ 1, 2 and 3) were observed before, but the fourth is a site not assigned in the original crystal structures of yeast tRNA^{Phe} determined by our group (Jack *et al.*, 1977). The 2.0 Å resolution of the electron density map, as well as their low temperature factors, permits the water structure of both the inner and outer hydration shells around the tightly bound Mg²⁺ to be resolved rather than inferred on the basis of difference maps as was the case for the lower resolution structures. Consequently, the present map provides a more detailed understanding of the ligation of magnesium ions to RNA and gives insights into their role in nucleic acid folding.

Magnesium site 1 is sandwiched between U8, A9 and C11, U12 in the D arm (Figure 3(a)). This site is created by the two triple base-pairs U8 and U9 form with the D stem. The Mg²⁺ contacts phosphate oxygen atoms of the four nucleotides (Mg²⁺ 1-O2P(U8) = 4.34 Å; Mg²⁺ 1-O1P, O2P(A9) = 5.43, 4.73 Å; Mg²⁺ 1-O2P(C11) = 4.60 Å; Mg²⁺ 1-O2P(U12) = 3.00 Å) *via* a set of water molecules that fill up its binding pocket, allowing the four phosphate groups to approach each other closely.

The Mg²⁺ at site 2 (Figure 3(b)) is located in the sharp turn between G20 and A21. The ion sits between their extremely closely spaced phosphate groups (P-P distance = 3.02 Å) so that, by making direct contact with their oxygen atoms (Mg²⁺ 2-O1P(G20) = 1.87 Å; Mg²⁺ 2-O2P(A21) = 2.04 Å), it stabilises the turn. Several such sites are also found in the structure of the *Tetrahymena* group I intron P4-P6 domain (Cate *et al.*, 1996). Two water molecules directly bound (1.92, 2.17 Å) to this metal ion are also visible (Figure 3(b)).

The Mg²⁺ at site 3 (Figure 3(c)) has one of the lowest temperature factors within the structure (29.6 Å²) and its inner, somewhat distorted pentahydrated shell is clearly discernible (in all cases, inner hydration spheres were not constrained to have an ideal octahedral geometry). This magnesium ion sits in a deep pocket formed by the bringing together of G19-G20 of the D loop and U59-C60 of the TΨC loop. Four of the water molecules in the inner hydration shell contact bases directly (O6 and N7 of G20 (2.81, 2.68 Å), O4 of

U59 (2.33 Å), N3 and N4 of C60 (3.14, 3.01 Å)). The O1P phosphate oxygen atom of G19 is contacted directly (2.05 Å), replacing one of the water molecules in the inner shell, while the O2P of G20 (at 6.21 Å) is contacted *via* a water molecule of the second hydration shell. Other water molecules in this region extend the number of contacts, permitting a complex network of interactions that fix the Mg²⁺ and also stabilise this part of the structure. The geometry of the magnesium binding is particularly interesting and is a recurring feature: two inner shell water molecules that contact the O6 and N7 of G20 (2.81, 2.68 Å) do so in a geometry mimicking a base-pair, while a third inner shell water located at about 60° from the Mg²⁺-guanine base plane contacts the O4 of U59 (2.33 Å) located on the ribose side of the G20 base (Figure 3(c)). Binding of Mg²⁺ to guanine bases through two inner water molecules has recently also been observed in structures of a 5 S rRNA domain (Correll *et al.*, 1997) and of sheared tandem G·A base-pairs (Gao *et al.*, 1999).

The same geometry of binding is also seen for Mg²⁺ site 4 (Figure 3(d)). This binding site is located at the junction between the D and anticodon arms and was not identified in the original 2.5 Å resolution structure by Hingerty and colleagues (Hingerty *et al.*, 1978; Brown *et al.*, 1985), although it was later suggested by Westhof & Sundaralingam (1986). It is also close to where a spermine molecule had been assigned in a previous analysis (Quigley *et al.*, 1978). In this case too, the density for the magnesium, its inner hydration shell and other associated water molecules is unambiguously resolved. The six water molecules in the inner hydration shell with slightly distorted octahedral geometry can be seen clearly (Figure 3(d)). In the manner seen at site 3, two inner water molecules “base-pair” with the O6 and

N7 of G42 (2.58, 3.08 Å) and a third water molecule, at about 70° to the Mg²⁺-guanine base plane, hydrogen bonds to the O4 of U41 (2.72 Å). In this instance, however, the uridine base is located on the non-ribose side of the G42 base. A fourth inner shell water is hydrogen bonded to one of the phosphate oxygen atoms of C25 (2.85 Å) and outer hydration water molecules contact G24, M2G26 and G43.

There is clear density for a spermine molecule sandwiched between two tRNA molecules in the crystal lattice (Figures 1 and 4). The spermine sits in the major groove of the TΨC arm and loop, with its N10 involved in a long-range interaction with O4 of U52 (3.83 Å) as well as water-mediated contacts with N7 and O1P of G51 (at 4.76 and 4.62 Å, respectively), the N5 hydrogen bonding to the O4 of 5MU54 and contacting both phosphate oxygen atoms of 1MA58 (3.28, 3.67 Å), the N1 interacting with the O2 of PSU55 (3.45 Å) as well as with the phosphate groups of G57 (3.49 Å), 1MA58 (3.82 Å) and A14 (3.24 Å) of a symmetry-related molecule. Spermine was a crucial component of the crystallisation buffer and its location explains its role in packing molecules in the crystal lattice, which is further stabilised by the interaction of the terminal A76 with A36 of the adjoining molecule by a single amino-N1 hydrogen bond.

Mg²⁺-catalysed tRNA hydrolysis in the crystal

Since the crystals were old and the electron density seemed poor for part of the D and anticodon loops, we decided to analyse the tRNA present in the batch of crystals used for data collection. The crystals, which were grown in dialysis bags as described in Materials and Methods, were recovered and washed several times in dialysis buffer. They were then dissolved and analysed by dena-

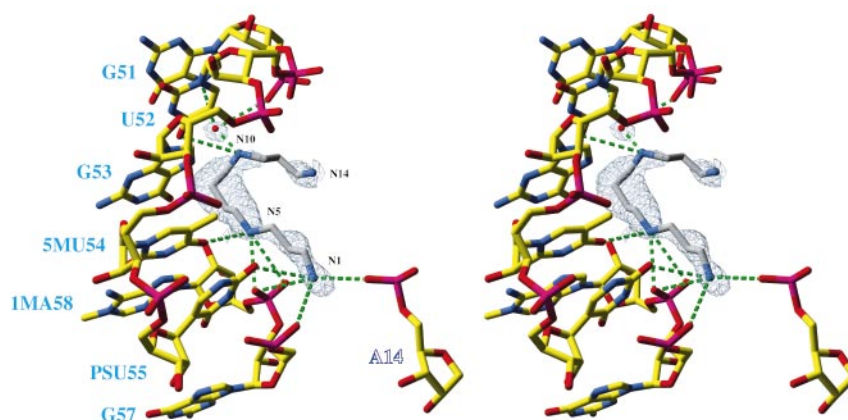


Figure 4. Stereo representation of the spermine molecule binding site. tRNA nucleotides, in stick representation, are colour-coded according legend to Figure 2; nitrogen and carbon atoms of spermine are shown in blue and grey, respectively. Nucleotide labels are colour-coded according legend to Figure 1(a). The combined, sigma-weighted $|2F_o - F_c|$ electron density map of spermine and of a water molecule mediating its interaction with nucleotide G51 is shown (contour = 0.9 σ). Contacts between spermine and RNA are indicated by broken green lines. The base of nucleotide A14 from a symmetry related molecule (labelled in reverse colour) has been omitted for clarity.

turing gel electrophoresis (Figure 5(a)). The analysis shows that about 40% of yeast tRNA^{Phe} in the crystals is cleaved at four positions clustered in two specific regions of the tRNA chain, resulting in eight main products: two complementary pairs of fragments of 15/16 and 61/60 nucleotides in length and another two pairs of fragments of 35/36 and 41/40 nucleotides. Self-cleavage in crystals

has also been observed for yeast tRNA^{Asp} (Moras *et al.*, 1985). Since the yeast tRNA^{Phe} crystals grew relatively rapidly (within a few days) and the starting material had been intact at the beginning of the experiment (data not shown), as also seen for our reference yeast tRNA^{Phe} marker (Figure 5(a), right lane), the site-specific hydrolysis observed must have occurred after the crystals had grown. The

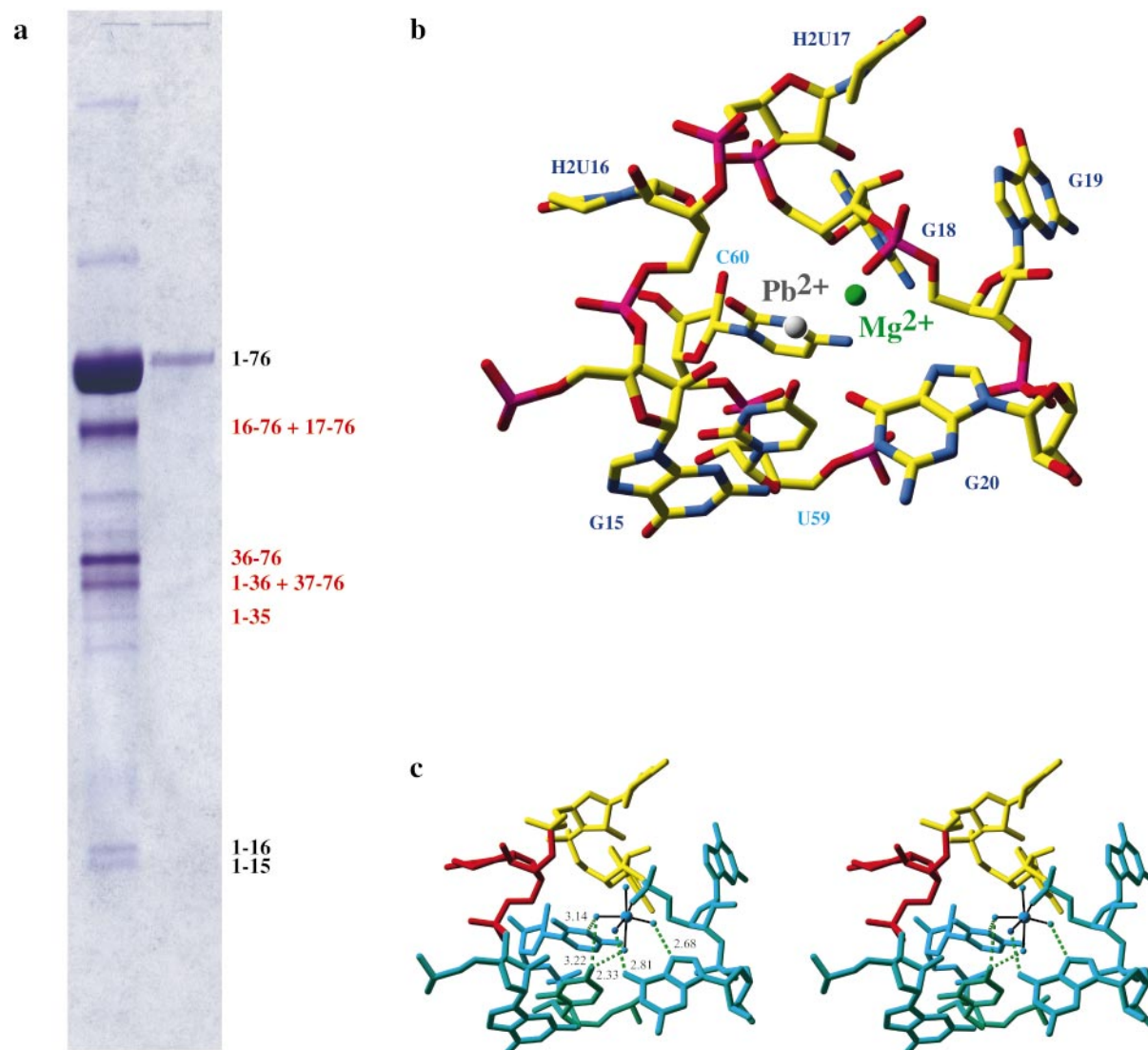


Figure 5. Mg²⁺-dependent hydrolysis of yeast tRNA^{Phe} in the crystals. (a) Denaturing gel electrophoresis analysis of tRNA^{Phe} recovered from 15 year old crystals from the same batch used for X-ray data collection. The tRNA from the crystals (left lane) is compared to a new batch of intact tRNA^{Phe} (SIGMA) (right). The identity of the major bands is indicated: bands 1-15 and 1-16 were assigned directly by MALDI-TOF; bands labelled in red have been interpreted by comparing their migration in the gel to that of bands 1-15, 1-16, full length tRNA^{Phe} and RNA markers of different sizes (21-32-43-58 nucleotides, not shown). (b) Relative positions of Pb²⁺ site 1 (grey) taken from the crystal at pH 5.0 (Brown *et al.*, 1983) and Mg²⁺ site 3 in the present structure (green) located in the binding pocket formed by the D loop and TΨC loop. The two metals occupy different positions located 2.5 Å apart. The binding of Mg²⁺ excludes binding of the Pb²⁺. Conventions are as in Figure 2. (c) Stereo-view of Mg²⁺ site 3 in the same orientation as in (b), colour-coded according to the relative temperature factors of the binding pocket. Note the high flexibility of nucleotides 16-18, and particularly of the first dihydrouridine, compared to that of the other nucleotides and of the Mg²⁺ itself. Broken green lines indicate hydrogen bonds, with distances in Å. For clarity, only water molecules directly bound to the metal ion are shown.

length of the fragments suggests that cleavage has taken place in the D loop and in the anticodon loop. This observation is consistent with an analysis of Mg²⁺-dependent hydrolysis of yeast tRNA^{Phe} carried out in solution at high pH conditions (pH 9.5), where the predominant cleavage of the ribose-phosphate chain occurred between H2U16 and H2U17 and, to a lesser extent, in the anticodon loop, resulting in half molecules (Wintermeyer & Zachau, 1973). Furthermore, the possibility of a Mg²⁺-catalysed cleavage of the phosphodiester bond between H2U16 and H2U17 was also inferred from the electron density map of the orthorhombic form of the tRNA^{Phe} crystals (Sussman *et al.*, 1978). To confirm the size of the fragments and hence the sites of hydrolysis that had occurred in our crystals, we analysed the tRNA recovered from the crystals by MALDI-TOF mass spectrometry. The molecular masses obtained (4985.2 and 5292.0 Da; see Materials and Methods) are consistent with cleavage having taken place between G15 and H2U16 and between H2U16 and H2U17. Unfortunately, the analysis did not give reliable information on the longer fragments and their direct determination could not be pursued further due to the scarcity of material recovered from the original crystals.

Since spontaneous hydrolysis of phosphodiester bonds in RNA is very slow, in the order of 1500 years (Li & Breaker, 1999), the hydrolysis we observe in the crystal over 15 years presents a modest rate increase of about 100-fold, providing evidence for a role for Mg²⁺ in the cleavage reaction, as well as pinpointing the sites of cleavage. Interestingly, the positions of the magnesium-dependent cleavage in the D loop (after G15 and H2U16) are respectively two and one nucleotides 5' to the well-characterised lead cleavage site between residues H2U17 and G18, observed both in solution and in the crystal (Brown *et al.*, 1983, 1985). The difference in the sites of hydrolysis provides evidence that cleavage is due to the presence of magnesium rather than small amounts of contaminating lead. Furthermore, metal content analysis of the crystallisation buffer revealed no presence of lead (see Materials and Methods). However, as the extent of Mg²⁺-dependent cleavage is low and the electron density for this flexible region rather poor, we were unable to resolve the cleaved structure in the electron density map. In Figure 5(b), the location of the Pb²⁺ in the lead crystal structure before hydrolysis (at pH 5.0; Brown *et al.*, 1985) is shown superimposed on the location of the Mg²⁺ (site 3) in the D/TΨC loop pocket of the present structure of yeast tRNA^{Phe}. The two metal ions are not located in the same position, but at a distance of about 2.5 Å from each other (Jack *et al.*, 1977; Brown *et al.*, 1985). Thus, the difference in the location of the metal ions in the binding pocket correlates with the difference in the resulting cleavage positions. For both metal ions, the phosphodiester bonds that undergo cleavage are located in a short, single stranded region

containing the two dihydrouridine groups, H2U16 and H2U17. The structure colour-coded according to temperature factors (Figure 5(c)) shows that the chain containing H2U16 and H2U17 is particularly flexible, having considerably higher temperature factors (average *B* factor ~61 Å²) than those of the tightly bound Mg²⁺ (29.6 Å²) and of the RNA chains to which the ion binds at the bottom of the binding pocket. The cleavage positions within the D loop in the magnesium crystal structure (Figure 5(a)) correlate well with the high temperature factor of H2U16, whereas the different location of the Pb²⁺ results in a shift of the cleavage site to the bond after H2U17, which is also relatively mobile. For Pb²⁺-dependent cleavage, the evidence points towards a metal hydroxide participating in alkaline hydrolysis because the p*K*_a value of Pb²⁺-bound waters is around 8 (Feig & Uhlenbeck, 1999) and RNA hydrolysis is rapid at neutral pH conditions and is much reduced at pH 5.0 (Brown *et al.*, 1985). The Pb²⁺ is located at ~6.4 Å from the O2' of the ribose of H2U17 that needs to be activated for nucleophilic attack to take place. The Mg²⁺ is also located far from the cleaved phosphodiester bonds (Mg²⁺ 3-O2'(G15) = 6.22 Å; Mg²⁺ 3-O2'(H2U16) = 9.13 Å). However, we note that one of the inner hydration water molecules points towards these bonds (H₂O-O2'(G15) = 5.25 Å; H₂O-O2'(H2U16) = 7.94 Å). Although the p*K*_a value of water molecules in the hydration shell of a Mg²⁺ is approximately 11 (Feig & Uhlenbeck, 1999), consistent with a much slower hydrolysis rate, it is possible that the p*K*_a value of this water could be lowered by the interactions between inner hydration shell waters. Another possibility is that nucleotide C60, whose N3 contacts the Mg²⁺ through the same inner shell water molecule (N3(C60)-H₂O = 3.14 Å; Figure 5(c)), participates in the self-cleavage reaction by acting as a general acid, while an hydrated metal hydroxide, resulting from splitting of the water molecule into OH⁻ and H⁺ upon protonation of N3(C60), would function as the general base. This second mechanism would be very similar to that recently proposed for a hepatitis delta virus ribozyme (Nakano *et al.*, 2000).

Whatever the mechanism, the most plausible rationale for site-specific hydrolysis is that the flexibility of the H2U16-G18 region allows sampling of different conformations, bringing the scissile bonds sufficiently close to the attacking group and in the right geometry for hydrolysis to take place. In order to reach this conformation, significant local "breathing" of the structure within the crystal would be required. These considerations suggest that a conformation compatible with the in-line attack mechanism (Soukup & Breaker, 1999) could in principle be achieved due to the local flexibility of the RNA. Consistent with this observation, flexibility is also important in the cleavage mechanism of the lead-dependent ribozyme (Wedekind & McKay, 1999).

The other major positions of cleavage are located within the anticodon loop, most likely between

A35 and A36 and between A36 and YG37 (Figure 5(a)), in another region of the structure with high temperature factors (Figure 1(c)). The mechanism for these cleavage reactions is even more obscure, but is unlikely to be due to non-specific metal promoted degradation since cleavage appears to be site-specific and in one case coincides with a clearly visible Mg²⁺ (Mg²⁺ 6) bound to the phosphate group of A36.

In summary, in tRNA as in ribozymes, Mg²⁺ can provide the right geometric environment and the positioning of groups for RNA self-cleavage to occur, whereas the inherent flexibility of the scissile bond allows it to adopt the geometry required for hydrolysis to take place.

Conclusions

We have taken advantage of the new generation of high energy X-ray sources and modern refinement techniques to re-determine the crystal structure of yeast tRNA^{Phe} to 2.0 Å resolution. The new structure is at a higher resolution than has so far been obtained for large, complex RNA structures. It corroborates much of the old structural information but reveals some novel details. The quality of the electron density allows the water structure around the magnesium ions to be directly resolved in the $|2F_o - F_c|$ map, providing a more precise understanding of the important role metal ions and their associated water molecules play in the folding and stabilisation of the structure of tRNAs.

Materials and Methods

tRNA preparation and crystallisation

Saccharomyces cerevisiae tRNA^{Phe} was purchased from Boehringer-Mannheim Corporation and further purified on a Sephadex G-100 gel filtration column equilibrated against 20 mM Tris-HCl (pH 7.5), 2 mM EDTA, 100 mM NaCl. The main peak was collected, precipitated and resuspended in 20 mM Tris-HCl (pH 7.5), 1 mM EDTA at a final concentration of 8 mg/ml. Monoclinic crystals were grown at 4 °C by dialysis of the tRNA at 4 mg/ml against 10 mM Tris-HCl (pH 7.5), 12 mM MgCl₂, 2 mM spermine and 6% (v/v) 1,6-hexanediol, essentially as described by Ladner *et al.* (1972). The crystals used for the crystallographic and biochemical analyses described in this paper had been stored at 4 °C and were about 15 years old.

Analysis of the cleavage of yeast tRNA^{Phe} in the crystals

Electrophoretic analysis

Crystals were transferred to a microtube and centrifuged at 13,600 g for five minutes, after which the mother liquor was removed. They were then washed five times with 500 µl of dialysis buffer and finally dissolved in 100 µl of 10 mM Tris-HCl (pH 7.0), 20 mM EDTA. RNA fragments were separated on denaturing polyacrylamide gels (10% 19:1 acrylamide:bis-acrylamide, 8 M urea, 1 × TBE) and stained with 0.1% (w/v)

toluidine blue. After drying, gels were scanned and analysed with the gel Plotting Macros of the public domain NIH Image program (developed at the US National Institutes of Health and available at <http://rsb.info.nih.gov/nih-image/>). Fragments deriving from cleavage at nucleotides H2U16 and H2U17 were identified by MALDI-TOF mass spectrometry (see below). Sizes of all other tRNA cleavage products were extrapolated from the migration of the dihydrouridine cleavage bands themselves, RNA markers of known composition of 21-32-43-58 nt, and full length yeast tRNA^{Phe}, which was fitted with a quasi-Newton algorithm in the program MacCurveFit (<http://www.home.aone.net.au/krs/mcf.html>), using the function $F(X) = a + b \times X^c$ ($a = 26.326$, $b = -7.441$, $c = 0.116$, $SSE = 0.028$, $R^2 = 0.997$).

MALDI-TOF mass spectrometry

To remove excess salts, tRNAs extracted from the crystals were precipitated with 2.5 volumes EtOH 96% (v/v)/0.1 volumes 3.3 M KOAc (pH 5.8) at -70 °C; pellets were washed with EtOH 70%, air dried and resuspended in Milli-Q H₂O. Alternatively, samples were desalted by drop dialysis against water using Millipore VS 0.025 µm filters. The resulting material (approximately 0.7 mg/ml) was prepared 1:1 with a solution of 3-hydroxypicolinic acid (25 mg/ml) in 70:30 acetonitrile-water containing diammonium hydrogen citrate (35 mg/ml). Calibration was by means of an internal DNA standard. Spectra were recorded using a Voyager DE mass spectrometer (PerSeptive Biosystems) in positive ion mode, using an accelerating voltage of 25 KV and a pulse delay time of 600 ns. Clear signals were recorded for RNA species with molecular masses of 4985.2 and 5292.0 Da, respectively; these figures are in excellent agreement with the expected masses of the small fragments resulting from cleavage between G15 and H2U16 (nt 1-15; 4947 Da) and between H2U16 and H2U17 (nt 1-16; 5255.2 Da), with the addition of a single potassium ion.

Trace metal analysis of crystallisation solution

Inductively coupled plasma emission spectroscopy (ICP-ES) analysis of the concentration of divalent metal ion contaminants in the crystallisation solution was performed at Butterworth Laboratories Limited, Teddington, UK. The concentrations of Mn, Ni, Zn, Pb and Cd ions were all below detectability (<0.5 mg/l).

Crystal cryoprotection and data collection

Crystals were first washed in fresh crystallisation solution at 4 °C for ten minutes and then cryoprotected at the same temperature by stepwise addition of 2-methyl-2,4-pentanediol (+5%/ten minutes) in the crystallisation buffer to a final concentration of 30%. They were then flash-frozen in liquid N₂ and stored for data collection. Several crystals were screened both at beamline 5.2R of Elettra synchrotron, Trieste, and beamline ID14-4 of ESRF synchrotron, Grenoble; of these, only one diffracted beyond 2.0 Å resolution and was used for data collection at 100 K at ESRF. The data set was indexed and integrated with Denzo, scaled and reduced with Scalepack (Otwinowski & Minor, 1997) and finally merged using the SCALE_NATIVE routine of Solve (Terwilliger & Berendzen, 1999). Although diffraction

spots could be observed to ~ 1.8 Å resolution, the $(I/\sigma(I))$ significantly dropped beyond 2.0 Å, which was then chosen as high resolution limit for processing (at this resolution, $(I/\sigma(I)) > 2$). Data processing statistics may be found in Table 1.

Refinement

As a result of the cryoprotection, the unit cell of the yeast tRNA^{Phe} crystals shrunk by more than 4% relative to the dimensions reported for the same crystal form for data collected at -5°C (PDB ID 4TNA; Hingerty *et al.*, 1978) and at 16°C (PDB ID 1TRA; Stout *et al.*, 1978; Westhof & Sundaralingam, 1986). Four rounds of rigid-body refinement were therefore performed with CNS (Brünger *et al.*, 1998) in order to get the correct starting orientation of the molecule within the cryo-cooled unit cell. The last available refined structure of monoclinic tRNA^{Phe} (1TRA, 3.0 Å resolution; Westhof & Sundaralingam, 1986) was used as starting model, since it yielded the best starting R and R_{free} values in a preliminary test where the 1TRA and 4TNA tRNA^{Phe} coordinates were compared using a common high resolution limit of 3.0 Å. In the first round, the whole tRNA molecule (including the five magnesium ions identified by Westhof & Sundaralingam (1986)) was refined as a rigid body against data up to 2.7 Å resolution. In the second round, three rigid bodies, respectively corresponding to (1) nt 1-7 and 49-76, (2) nt 8-48; and (3) Mg²⁺, were defined and independently refined to the same resolution. In the third round, the number of rigid units was increased to 20 ((1): nt 1-7, 66-72; (2): nt 73; (3): nt 49-53, 61-65; (4): nt 8; (5): nt 9; (6): nt 54-60; (7): nt 10-13, 22-25; (8): nt 14-21; (9): nt 26; (10): nt 27-31, 39-43; (11): nt 32-38; (12): nt 44; (13): nt 45; (14): nt 46; (15): nt 47; (16): nt 48; (17): nt 74; (18): nt 75; (19): nt 76; (20): Mg²⁺ ions). In the last round, the tRNA molecule was again refined as a single rigid body, while each of the Mg²⁺ was independently refined. At this stage, the crystallographic R value was 35.4% and the R_{free} value was 37.1% for all data up to 2.7 Å resolution. The refinement was then continued by alternating rounds of manual rebuilding with the program O (Jones & Kjeldgaard, 1997) and energy minimisation with CNS (Brünger *et al.*, 1998), while gradually including high resolution reflections up to 2.0 Å. Both sigma-weighted $|F_o - F_c|$ difference maps and composite annealed omit maps (Brünger *et al.*, 1997) were inspected during rebuilding. These maps were particularly useful to correct the sugar puckering of nucleotides A21 and U47 and confirm introduction of water molecules in correspondence of unaccounted $|2F_o - F_c|$ map density peaks. In addition, electron density maps were also calculated using X-ray holographic image reconstruction, a real-space electron density imaging and refinement procedure implemented in the program EDEN (Szöke, 1993; Somoza *et al.*, 1995; Szöke *et al.*, 1997 (http://www.dl.ac.uk/CCP/CCP4/proceedings/1997/a_szoke/main.html)). For holographic reconstructions in both correction and completion mode, a solvent target was prepared using the rigid-body refined yeast tRNA^{Phe} model to construct a low-resolution solvent mask, which was then used with weights of 0.01-0.001. The solvent structure of tRNA^{Phe} was completely rebuilt using conservative criteria, so that water molecules were fitted only in density peaks above 1.0 σ in the $|2F_o - F_c|$ and composite anneal omit maps, spaced by a maximum of 3.8 Å (= 3.5 Å + expected coordinate error) from either RNA atoms or other water molecules. Throughout refinement, a maximum likelihood target was used and

bulk solvent and overall anisotropic B factor corrections were applied. Nucleotide bases were restrained to be planar; no restraints were specified for Mg²⁺ octahedral coordination. Individual B factor refinement of all RNA atoms was performed; alternated rounds of individual B factor and occupancy refinement of all Mg²⁺, spermine and water molecules were also carried out until convergence. Within the D loop, density for most of nucleotide H2U16 (with the exception of the phosphate group and the O5' atom), as well as for the phosphate group, O5' and C5' atoms of H2U17, was very poor. Since gel analysis of tRNA from the crystals indicated partial cleavage at either side of H2U16, the individual occupancy of the atoms in this region was also refined. While the final maps show clear density for both the ribose and the base of nucleotide H2U17, the position of H2U16 could not be unambiguously resolved and its current coordinates should therefore be considered tentatively. All Mg²⁺ sites identified in the monoclinic crystals by Hingerty *et al.* (1978) (PDB ID 4TNA) and Westhof & Sundaralingam (1986) (PDB ID 1TRA) are confirmed by the high resolution structure, with the exception of Mg²⁺ 4 of entry 4TNA and Mg²⁺ 5 of entry 1TRA. Mg²⁺ site 4 of the orthorhombic crystal structure of tRNA^{Phe} (PDB ID 4TRA; Westhof *et al.*, 1988a) is also not observed in the current model. The RMSDs between our final model and entries 4TNA, 1TRA and 4TRA (excluding nucleotide H2U16, ion, spermine and water atoms) are 1.09 Å, 1.14 Å and 1.16 Å, respectively (superpositions and RMSD calculations were performed using the McLachlan algorithm (McLachlan, 1982), as implemented in the program ProFit (Martin, A. C. R., <http://www.biochem.ucl.ac.uk/~martin/programs/#profit1>)).

Figure 1(b) was produced using Ribbons (Carson, 1997); Figures 1(c), 2, 3, 4, 5(b) and (c) were prepared with Swiss-PdbViewer (Guex & Peitsch, 1997) and POV-Ray[®] (<http://www.povray.org>).

Coordinates and structure factors

Atomic coordinates and structure factors have been deposited in the Nucleic Acid Database (accession code TR0002) and in the Protein Data Bank (PDB) (accession code 1EVV). They are also accessible at <http://www.mssm.edu/students/jovinl02/research/research.html>

Note added in proof

A high resolution crystal structure of yeast tRNA^{Phe} has also been independently determined by the group headed by Professor Peter B. Moore (Shi & Moore (2000). RNA, in the press).

Acknowledgements

We thank Titia Sixma and Katjusa Brejc (NKI, Amsterdam) for beamtime and help during data collection at ESRF; David Earnshaw (MRC-LMB, Cambridge) and Scott Furey (Chemistry Department, University of Cambridge) for help with MALDI-TOF analysis; Navraj Pannu and Randy Read (MRC Dunn Human Nutrition Unit, Cambridge) for advice on CNS; Patrick Gendron and François Major (Department of Computer Sciences and O.R., University of Montreal) for RNA conformation analysis with the program Annotate (Gendron, Lemieux

& Major, <http://www-lbit.iro.umontreal.ca/mcsym/>; Aaron Klug, Kiyoshi Nagai, Chris Oubridge, Brian Wimberly, Mike Gait, Roger Williams (MRC-LMB, Cambridge), Eric Westhof (CNRS, Strasbourg), William G. Scott (UCSC) and one anonymous referee for many useful comments.

References

- Auffinger, P. & Westhof, E. (1997). RNA hydration: three nanoseconds of multiple molecular dynamics simulations of the solvated tRNA^{Asp} anticodon loop. *J. Mol. Biol.* **269**, 326-341.
- Brown, R., Hingerty, B., Dewan, J. & Klug, A. (1983). Pb(II)-catalysed cleavage of the sugar-phosphate backbone of yeast tRNA^{Phe} - implications for lead toxicity and self-splicing RNA. *Nature*, **303**, 543-546.
- Brown, R., Dewan, J. & Klug, A. (1985). Crystallographic and biochemical investigation of the lead(II)-catalysed hydrolysis of yeast phenylalanine tRNA. *Biochemistry*, **24**, 4785-4801.
- Brünger, A. T., Adams, P. D. & Rice, L. M. (1997). New applications of simulated annealing in X-ray crystallography and solution NMR. *Structure*, **5**, 325-336.
- Brünger, A. T., Adams, P. D., Clore, G. M., DeLano, W. L., Gros, P., Grosse-Kunstleve, R. W., Jiang, J. S., Kuszewski, J., Nilges, M., Pannu, N. S., Read, R. J., Rice, L. M., Simonson, T. & Warren, G. L. (1998). Crystallography and NMR system: a new software suite for macromolecular structure determination. *Acta Crystallog. sect. D*, **54**, 905-921.
- Carson, M. (1997). Ribbons. *Methods Enzymol.* **277**, 493-505.
- Cate, J. H., Gooding, A. R., Podell, E., Zhou, K., Golden, B. L., Kundrot, C. E., Cech, T. R. & Doudna, J. A. (1996). Crystal structure of a group I ribozyme domain: principles of RNA packing. *Science*, **273**, 1678-1685.
- Cate, J. H., Hanna, R. L. & Doudna, J. A. (1997). A magnesium ion core at the heart of a ribozyme domain. *Nature Struct. Biol.* **4**, 553-558.
- Cech, T. R. & Uhlenbeck, O. C. (1994). Hammerhead nailed down. *Nature*, **372**, 39-40.
- Correll, C. C., Freeborn, B., Moore, P. B. & Steitz, T. A. (1997). Metals, motifs, and recognition in the crystal structure of a 5S rRNA domain. *Cell*, **91**, 705-712.
- Feig, A. L. & Uhlenbeck, O. C. (1999). The role of metal ions in RNA biochemistry. In *The RNA World* (Gesteland, R. F., Cech, T. R. & Atkins, J. F., eds), 2nd edit., pp. 287-319, CSHL Press, Cold Spring Harbor, NY.
- Gao, Y.-G., Robinson, H., Sanishvili, R., Joachimiak, A. & Wang, A. H.-J. (1999). Structure and recognition of sheared tandem G·A base-pairs associated with human centromere DNA sequences at atomic resolution. *Biochemistry*, **38**, 16452-16460.
- Guex, N. & Peitsch, M. (1997). SWISS-MODEL and the Swiss-PdbViewer: an environment for comparative protein modelling. *Electrophoresis*, **18**, 2714-2723.
- Hingerty, B., Brown, R. & Jack, A. (1978). Further refinement of the structure of yeast tRNA^{Phe}. *J. Mol. Biol.* **124**, 523-534.
- Jack, A., Ladner, J. & Klug, A. (1976). Crystallographic refinement of yeast phenylalanine transfer RNA at 2.5 Å resolution. *J. Mol. Biol.* **108**, 619-649.
- Jack, A., Ladner, J. E., Rhodes, D., Brown, R. S. & Klug, A. (1977). A crystallographic study of metal-binding to yeast phenylalanine transfer RNA. *J. Mol. Biol.* **111**, 315-328.
- Jones, T. & Kjeldgaard, M. (1997). Electron-density map interpretation. *Methods Enzymol.* **277**, 173-208.
- Kim, S., Suddath, F., Quigley, G., McPherson, A., Sussman, J., Wang, A., Seeman, N. & Rich, A. (1974). Three-dimensional tertiary structure of yeast phenylalanine transfer RNA. *Science*, **185**, 435-440.
- Ladner, J. E., Finch, J., Klug, A. & Clark, B. (1972). High-resolution X-ray diffraction studies on a pure species of transfer RNA. *J. Mol. Biol.* **72**, 99-101.
- Ladner, J. E., Jack, A., Robertus, J. D., Brown, R., Rhodes, D., Clark, B. & Klug, A. (1975). Structure of yeast phenylalanine transfer RNA at 2.5 Å resolution. *Proc. Natl Acad. Sci. USA*, **72**, 4414-4418.
- Li, Y. & Breaker, R. R. (1999). Kinetics of RNA degradation by specific base catalysis of transesterification involving the 2'-hydroxyl group. *J. Am. Chem. Soc.* **121**, 5364-5372.
- McLachlan, A. (1982). Rapid comparison of protein structures. *Acta Crystallog. sect. A*, **38**, 871-873.
- Moras, D., Dock, A. C., Dumas, P., Westhof, E., Romby, P., Ebel, J. & Giegé, R. (1985). The structure of yeast tRNA^{Asp}. A model for tRNA interacting with messenger RNA. *J. Biomol. Struct. Dynam.* **3**, 479-493.
- Nakano, S., Chadalavada, D. M. & Bevilacqua, P. C. (2000). General acid-base catalysis in the mechanism of a hepatitis delta virus ribozyme. *Science*, **287**, 1493-1497.
- Otwinowski, Z. & Minor, W. (1997). Processing of X-ray diffraction data collected in oscillation mode. *Methods Enzymol.* **276**, 307-326.
- Quigley, G., Teeter, M. & Rich, A. (1978). Structural analysis of spermine and magnesium ion binding to yeast phenylalanine transfer RNA. *Proc. Natl Acad. Sci. USA*, **75**, 64-68.
- Rhodes, D. (1977). Initial stages of the thermal unfolding of yeast phenylalanine transfer RNA as studied by chemical modification: the effect of magnesium. *Eur. J. Biochem.* **81**, 91-101.
- Robertus, J. D., Ladner, J. E., Finch, J. T., Rhodes, D., Brown, R. S., Clark, B. F. C. & Klug, A. (1974). Structure of yeast phenylalanine tRNA at 3 Å resolution. *Nature*, **250**, 546-551.
- Scott, W. G. & Klug, A. (1996). Ribozymes: structure and mechanism in RNA catalysis. *Trends Biochem. Sci.* **21**, 220-224.
- Somoza, J. R., Szöke, H., Godman, D. M., Beran, P., Truckses, D., Kim, S.-H. & Szoke, A. (1995). Holographic methods in X-ray crystallography. IV. A fast algorithm and its application to macromolecular crystallography. *Acta Crystallog. sect. A*, **51**, 691-708.
- Soukup, G. A. & Breaker, R. R. (1999). Relationship between internucleotide linkage geometry and the stability of RNA. *RNA*, **5**, 1308-1325.
- Stout, C., Mizuno, H., Rao, S., Swaminathan, P., Rubin, J., Brennan, T. & Sundaralingam, M. (1978). Crystal and molecular structure of yeast phenylalanyl transfer RNA. Structure determination, difference Fourier refinement, molecular conformation, metal and solvent binding. *Acta Crystallog. sect. B*, **34**, 1529-1544.
- Sussman, J. L., Holbrook, S. R., Wade Warrant, R., Church, G. M. & Kim, S.-H. (1978) Crystal structure of yeast phenylalanine transfer RNA. I. Crystallographic refinement. *J. Mol. Biol.* **123**, 607-630.
- Szöke, A. (1993). Holographic methods in X-ray crystallography. II. Detailed theory and connection to

- other methods in crystallography. *Acta Crystallog. sect. A*, **49**, 853-866.
- Szoke, A., Szoke, H. & Somoza, J. R. (1997). Holographic methods in X-ray crystallography. *CCP4 Daresbury Study Weekend Proceedings*, 179-189.
- Terwilliger, T. C. & Berendzen, J. (1999). Automated structure solution for MIR and MAD. *Acta Crystallog. sect. D*, **55**, 849-861.
- Wedekind, J. E. & McKay, D. B. (1999). Crystal structure of a lead-dependent ribozyme revealing metal binding sites relevant to catalysis. *Nature Struct. Biol.* **6**, 261-268.
- Westhof, E. (1988). Water: an integral part of nucleic acid structure. *Annu. Rev. Biophys. Biophys. Chem.* **17**, 125-144.
- Westhof, E. & Sundaralingam, M. (1986). Restrained refinement of the monoclinic form of yeast phenylalanine transfer RNA. Temperature factors and dynamics, coordinated waters and base-pair propeller twist angles. *Biochemistry*, **25**, 4868-4878.
- Westhof, E., Dumas, P. & Moras, D. (1988a). Restrained refinement of two crystalline forms of yeast aspartic acid and phenylalanine transfer RNA crystals. *Acta Crystallog. sect. A*, **44**, 112-123.
- Westhof, E., Dumas, P. & Moras, D. (1988b). Hydration of transfer RNA molecules: a crystallographic study. *Biochimie*, **70**, 145-165.
- Wintermeyer, W. & Zachau, H. G. (1973). Mg²⁺ katalysierte, spezifische spaltung von tRNA. *Biochim. Biophys. Acta*, **299**, 82-90.

Edited by J. Karn

(Received 20 April 2000; received in revised form 6 June 2000; accepted 13 June 2000)

ERRATUM

The Crystal Structure of Yeast Phenylalanine tRNA at 2.0 Å Resolution: Cleavage by Mg²⁺ in 15-year Old Crystals

Luca Jovine, Snezana Djordjevic and Daniela Rhodes
J. Mol. Biol. (2000) 301, 401–414

It is regretted that Figure 4 of the above paper was printed incorrectly; it appears correctly below.

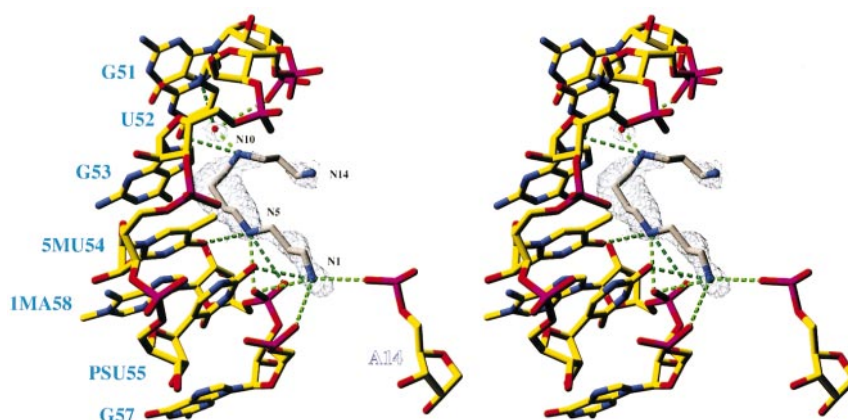


Figure 4. Stereo representation of the spermine molecule binding site. tRNA nucleotides, in stick representation, are colour-coded according legend to Figure 2; nitrogen and carbon atoms of spermine are shown in blue and grey, respectively. Nucleotide labels are colour-coded according legend to Figure 1(a). The combined, sigma-weighted $|2F_o - F_c|$ electron density map of spermine and of a water molecule mediating its interaction with nucleotide G51 is shown (contour = 0.9 σ). Contacts between spermine and RNA are indicated by broken green lines. The base of nucleotide A14 from a symmetry related molecule (labelled in reverse colour) has been omitted for clarity.